MEaSUREs InSAR-Based Antarctica Ice Velocity Map, Version 2

USER GUIDE

How to Cite These Data

As a condition of using these data, you must include a citation:

Rignot, E., J. Mouginot, and B. Scheuchl. 2017. *MEaSUREs InSAR-Based Antarctica Ice Velocity Map, Version 2*. [Indicate subset used]. Boulder, Colorado USA. NASA National Snow and Ice Data Center Distributed Active Archive Center. https://doi.org/10.5067/D7GK8F5J8M8R. [Date Accessed].

FOR QUESTIONS ABOUT THESE DATA, CONTACT NSIDC@NSIDC.ORG

FOR CURRENT INFORMATION, VISIT https://nsidc.org/data/NSIDC-0484

National Snow and Ice Data Center

TABLE OF CONTENTS

1   DETAILED DATA DESCRIPTION

1.1 Format

The data are formatted in Network Common Data Form, Version 4 (NetCDF-4) (.nc) following version 1.6 of the Climate and Forecast (CF) metadata conventions. For more information about working with NetCDF formatted data, visit the UCAR Unidata Network Common Data Form Web site.

1.2 File and Directory Structure

Data are available on the HTTPS site in the https://n5eil01u.ecs.nsidc.org/MEASURES/NSIDC-0484.002/ directory in one folder, 1996.01.01/. In this folder, there is one file: antarctica_ice_velocity_450m_v2.nc.

1.3 File Naming Convention

This data set includes one file named antarctica_ice_velocity_450m_v2.nc (450 m grid spacing).

1.4 File Size

The size of this data set is approximately 4 GB.

1.5 Spatial Coverage

The data set spans the continent of Antarctica. Figure 1 provides a map of the spatial coverage.

Southernmost Latitude: 90° S
Northernmost Latitude: 60° S
Westernmost Longitude: 180° W
Easternmost Longitude: 180° E
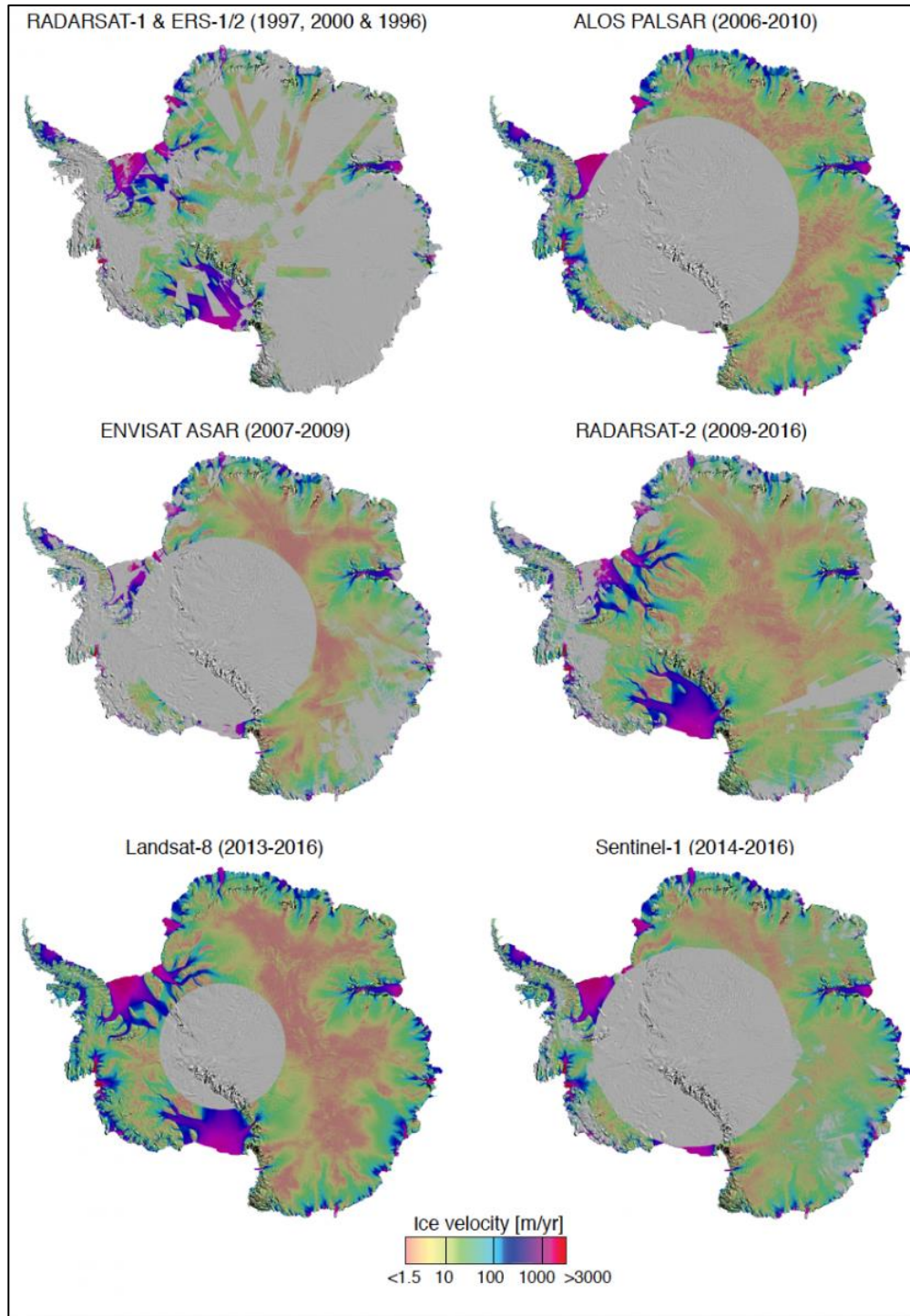
1.5.1   Spatial Coverage Map

Figure 1. Antarctic ice velocity derived from RADARSAT-1, ERS-1 and 2, ALOS PALSAR, ENVISAT ASAR, RADARSAT-2, Landsat-8, and Copernicus Sentinel-1, color-coded on a logarithmic scale and overlaid on a MODIS mosaic of Antarctica. Projection is polar stereographic at 71° S secant plane.

1.5.2   Spatial Resolution

The spatial resolution of the velocity map is 450 m.

1.5.3   Projection

Polar stereographic with true scale at 71° S. Refer to Polar Stereographic Projection and Grid page for more information and polar stereographic grid definitions.

1.6 Temporal Coverage

The data were collected between 1996 and 2016. Detailed information is provided in the 3 section.

1.7 Parameter or Variable

This data set provides a comprehensive ice velocity map of the Antarctic Ice Sheet posted at 450 m grid spacing. The velocity components for the x and y direction, as defined by the polar stereographic grid, are stored in the NetCDF variables named VX and VY and are recorded in m/yr. Error estimates for the velocity components are provided as variables ERRX and ERRY; however, these values should be used more as an indication of relative quality rather than absolute error. More information about the error estimates is provided in the 2.1 section as well as in Rignot, et al. 2011. The data also include the standard deviations for the velocity estimates (STDX,STDY), as well as a count of scenes (CNT) used to estimate the values for each pixel. Figure 2 shows the error and standard deviation estimates, and Figure 3 shows the total number of measurements used to estimate the velocity. Figure 4 shows a sample image of the data as a whole Table 1

provides a complete list of the variables and their descriptions.

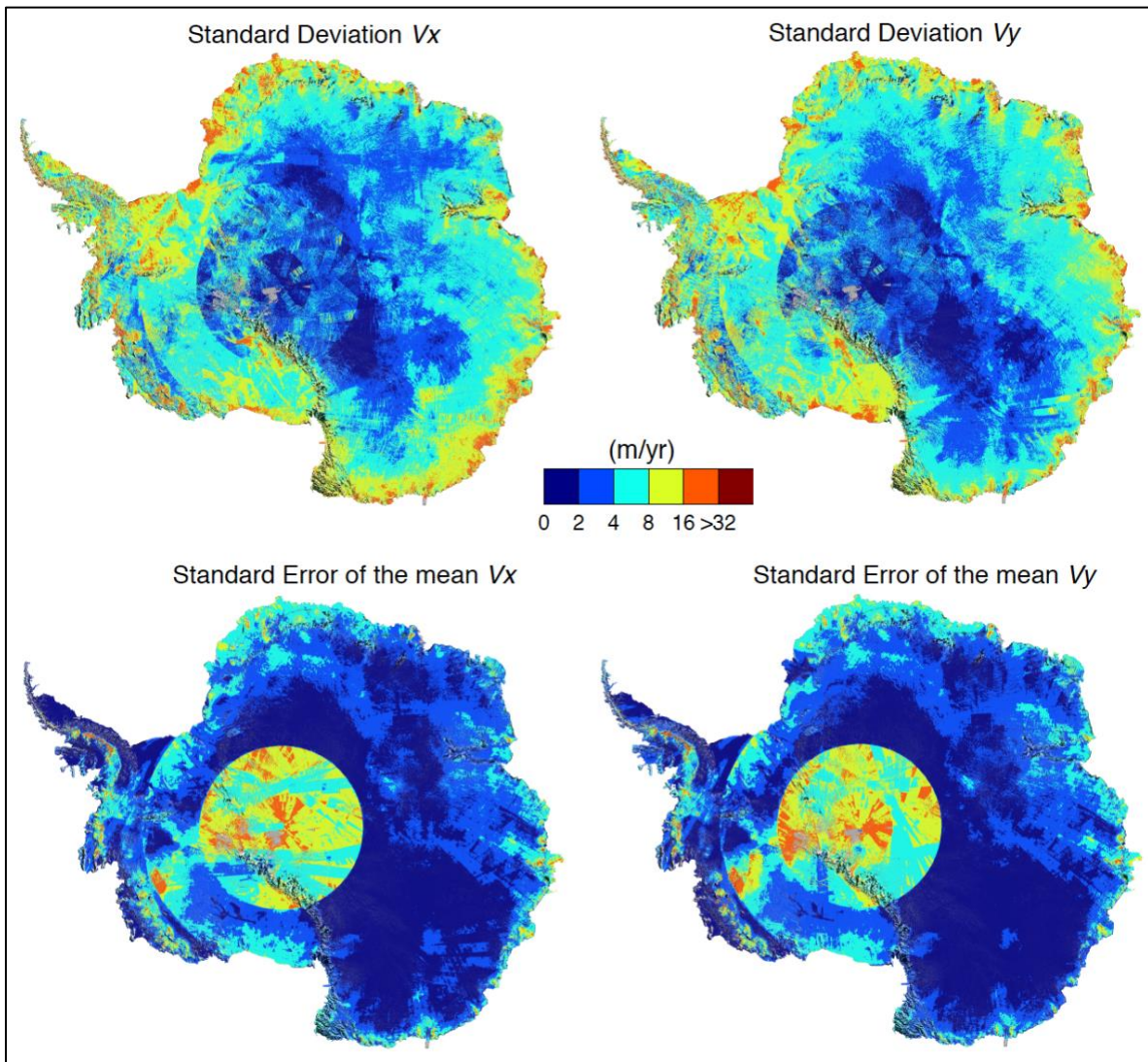Figure 2. Standard deviation of vx and vy (top row) and standard error of the mean vx and vy on a linear scale color-coded from 1 to greater than 32 m/yr
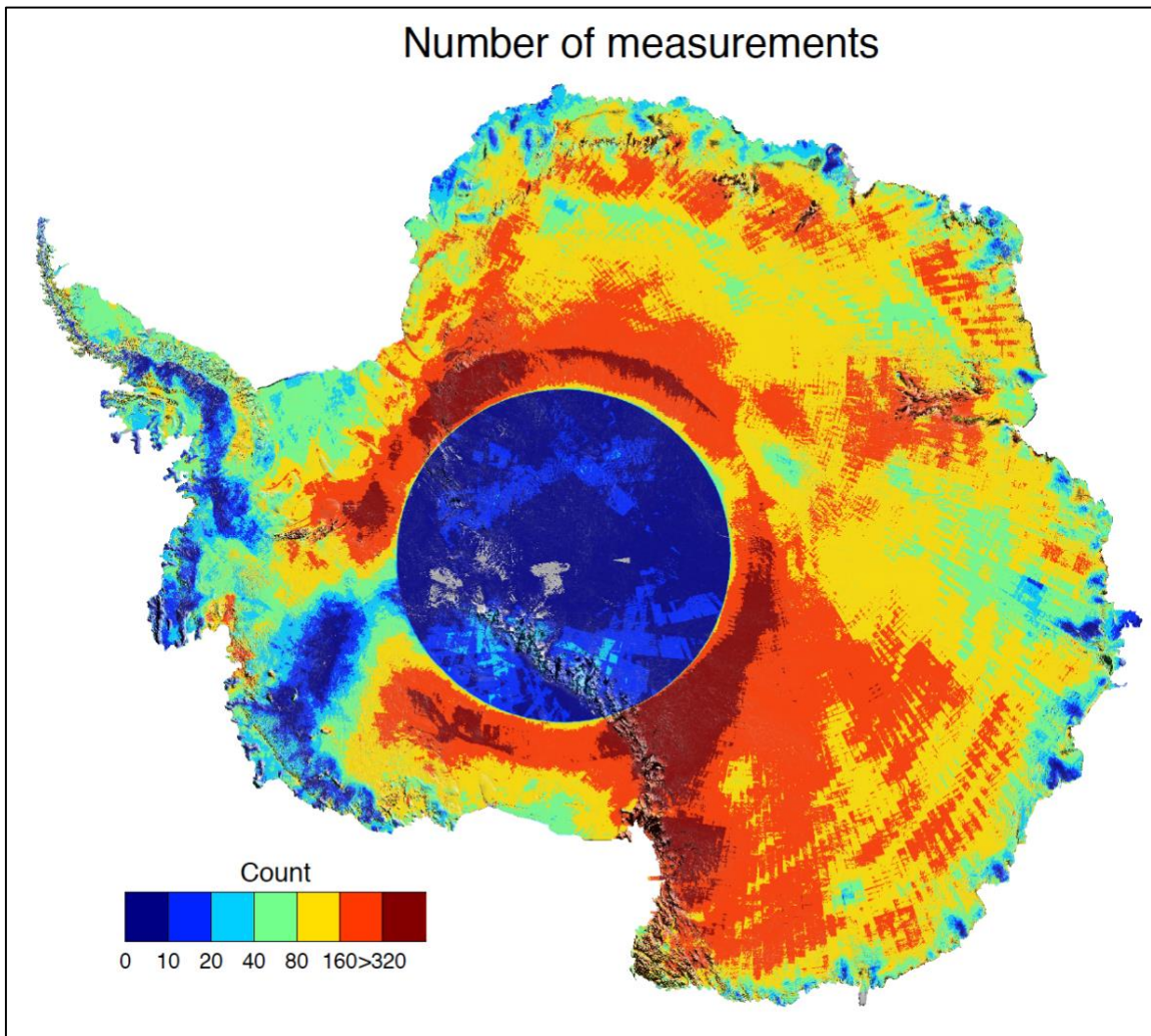
Figure 3. Number of measurements per pixel in the ice velocity mosaic (all sensors included)

1.7.1   Variable Description

The variables included in the NetCDF file are described in Table 1. All variables have grid dimensions of 12445 x 12445 and are posted at 450 m spacing.

Table 1. Variable Description

Variable	Description	Data Type
VX	Component of velocity in m/yr in x direction	float
VY	Component of velocity in m/yr in y direction	float
ERRX	Estimated error in m/yr in x direction	float
ERRY	Estimated error in m/yr in y direction	float
STDX	Standard deviation of vx	float
STDY	Standard deviation of vy	float
CNT	Count of scenes used per pixel	integer

To convert the VX and VY velocity components into magnitude (speed) and direction (angle), use the following equations:

(1) speed = $\sqrt{(vx2 + vy2)}$

(2) angle = arctan (vy / vx)

(3) error = $\sqrt{(errx2 + erry2)}$

(4) error of flow direction = error/(2*speed) (see Mouginot et al., 2012)

However, users should take care when computing the inverse tangent due to the function's inherent ambiguities. While the standard arctan function typically does not account for angles that differ by 180°, most modern computer languages and math software packages include the function ATAN2, which uses the signs of both vector components to place the angle in the proper quadrant.
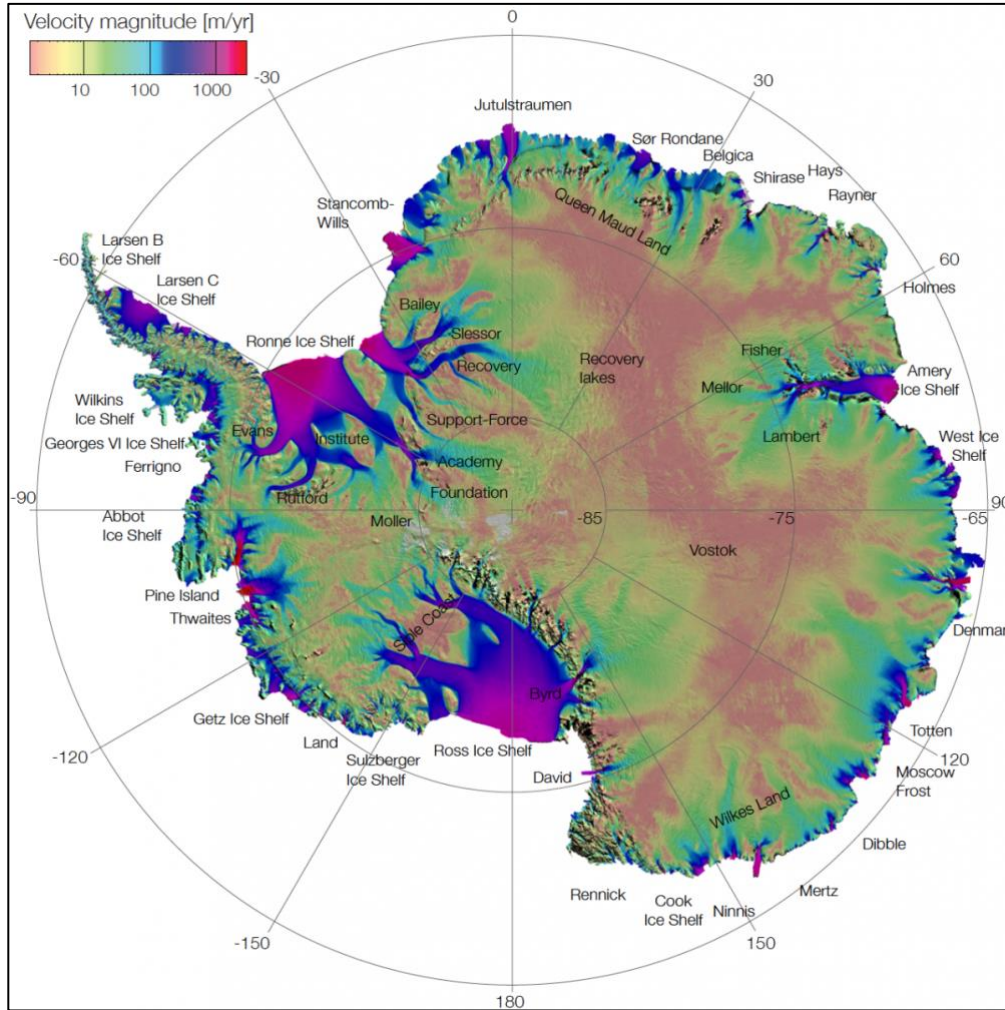
1.7.2 Sample Image

Figure 4. Antarctic ice velocity derived from RADARSAT-1, ERS-1 and 2, ALOS PALSAR, ENVISAT ASAR, RADARSAT-2, TerraSAR-X, TanDEM-X, Copernicus Sentinel-1, and Landsat-8, color-coded on a logarithmic scale.

2   SOFTWARE AND TOOLS

Unidata at the University Corporation for Atmospheric Research maintains an extensive list of freely available Software for Manipulating or Displaying NetCDF Data.

2.1 Quality Assessment

A detailed description of these data and their quality is provided in Rignot, et al., 2011. The precision of ice flow mapping varies with the sensor, the geographic location, the technique of interferometric analysis (refer to 3 for details), the time period of analysis, the repeat cycle, and the amount of data stacking. The error estimates are summarized in Table 2. The error map in Figure 2 takes into account the following error sources:

- Error of speckle tracking and interferometric phase analysis respectively (SAR only)
- Errors caused by ionospheric perturbations (strongest in the azimuth direction, stronger in L-band compared to C-band, stronger in the East Antarctic Ice Sheet (EAIS) compared to the West Antarctic Ice Sheet (WAIS) because ionospheric perturbations are more abundant near the magnetic pole
- Error of feature tracking analysis (Landsat-8 only)
- Data stacking (reduces the error noise as the square root of the number of interferometric pairs averaged)
- Respective weight of each instrument in the mosaicking

The total error is the square root of the sum of the independent errors squared. More details on the error estimates are provided in Mouginot, et al., 2017. Table 2 provides the error in ice velocity mapping for each sensor, without data stacking, in range (Rg) and azimuth (Az).

Table 2. Error in Ice Velocity Mapping (m/yr)

Platform/Sensor	Nominal Repeat Cycle (day)	Error (m/yr)	
		Rg	Az
ALOS (WAIS)/PALSAR	46	6	17
ALOS (EAIS)/PALSAR	46	6	5
ENVISAT/ASAR	35	21	4
RADARSAT-2/SAR	24	26	8
RADARSAT-1/SAR	24	26	8
Sentinel-1/SAR	12	12	43
Landsat-8/OLI	16	34*	34*
TanDEM-X (TDX)/TerraSAR-X (TSX)/SAR	11	8	8
Tandem ERS-1 and -2 (phase)/SAR	1	1	N/A

*Landsat uses repeat image feature tracking in x and y

3   DATA ACQUISITION AND PROCESSING

3.1 Theory of Measurements

This data set provides a comprehensive ice velocity map for the entire Antarctic ice sheet, derived from a variety of satellite radar interferometry data. (See the 3.2.1 section for a complete list.) Several analysis techniques using SAR data were used to generate the maps:

- Speckle tracking in both along (azimuth) and across (range) track directions
- Calculation of two dimensional offsets in amplitude imagery
- Combinations of (range) interferometric phases along two independent tracks
- Combination of interferometric phases of two independent tracks to retrieve the surface flow vector

In all cases, surface parallel flow is assumed, a conventional approach for ice sheets. The Landsat-8 data are processed using repeat image feature tracking (see Mouginot, et al. 2017).

3.2 Data Acquisition Methods

This digital image mosaic was built from the sources listed in 3.2.1, as well as the following:

- The RADARSAT-2 data acquired during spring 2009 was augmented by a 2011 gap-filling campaign
- Envisat Advanced Synthetic Aperture Radar (ASAR) data acquired during spring 2007, 2008, and 2009
- Advanced Land Observing Satellite (ALOS) Phased Array type L-band Synthetic Aperture Radar (PALSAR) data acquired during fall 2007-2008

The Version 2.0 mosaic also uses RADARSAT-2 (CSA) (2012-2016) and Sentinel-1 (Copernicus/ESA/EU) (2014-2016) data, Landsat-8 data acquired between 2013 and 2016, TanDEM-X and TerraSAR-X (DLR) between 2011 and 2014, and additional PALSAR (ALOS/JAXA) between 2006 and 2010. SAR acquisitions between 2006 and 2016 were coordinated by the IPY Space Task Group and its successor, the Polar Space Task Group (PSTG).

3.2.1 Data Sources

Table 3 describes the data sources used in this data set.

Table 3. Temporal and spatial coverage of source satellite data

Platform/Sensor	Space Agency	Look Dir.	Mode	Repeat Cycle (day)	Incidence Angle	Resolution Rg x Az (m)	Frequency (GHz)	Year
ERS-1 & 2/SAR	European Space Agency (ESA)	Right	N/A	1-3	23	13x4	5.33	1996
RADARSAT-1/SAR	Canadian Space Agency (CSA)	Left/Right	Varies	24	18-47	12x5-17x6	5.33	1997/2000
ENVISAT/ASAR	ESA	Right	IS2	35	23	13x5	5.33	2007-2009
RADARSAT-2/SAR	CSA	Left	S5/EH4	24	41/57	12x5	5.33	2009-2016
ALOS/PALSAR	Japan Aerospace Exploration Agency (JAXA)	Right	FBS	46	39	7x4	1.27	2006-2010
Sentinel-1/SAR	ESA	Right	IW-T OPS	12		12x43	5.33	2014-2016
Landsat-8/OLI	USGS/NASA	N/A	Panchromatic	16	N/A	15x15		2013-2016
TanDEM-X/TerraSAR-X/SAR	German Space Agency (DLR)	right	N/A	11	46.3	1.4x1.8	9.65	2011-2016

3.2.2 Version History

Version 2.0 was released April 2017. Refer to Table 4 for this data set's version history:

Table 4. Version History

Version	Description
V2.0	Added post 2011 SAR data (RADARSAT-2, Sentinel-1, TanDEM-X/TerraSAR-X) and Landsat-8 optical data (March 2017). The mosaicking method was updated to make best use of the large number of scenes used for the mosaic. New quality parameters including the standard deviation and count variables are provided in the NetCDF file.
V1.2	Binary data file format discontinued. Data available in NetCDF only (August 2015).
V1.1	Added a second mosaic at 450 m resolution (September 2013)
V1	Initial version (October, 2011)

3.3 References and Related Publications

Li, X., E. Rignot, M. Morlighem, J. Mouginot, and B. Scheuchl. 2015. Grounding line retreat of Totten Glacier, East Antarctica, 1996 to 2013. *Geophysical Research Letters* 42: 8049–8056. doi: 10.1002/2015GL065701.

Michel, R., and E. Rignot. 1999. Flow of Glacier Moreno, Argentina, from Repeat-Pass Shuttle Imaging Radar Images: Comparison of the Phase Correlation Method with Radar Interferometry. *Journal of Glaciology* 45(149): 93-100.

Mouginot, J., et al. 2017. Comprehensive Annual Ice Sheet Velocity Mapping Using Landsat-8, Sentinel-1, and RADARSAT-2 Data. *Remote Sensing 9(4):* Art. #364. doi: 10.3390/rs9040364.

Mouginot, J., E. Rignot, and B. Scheuchl. 2015. Sustained increase in ice discharge from the Amundsen Sea Embayment, West Antarctica, from 1973 to 2013. *Geophysical Research Letters* 41: 1576–1584. doi: 10.1002/2013GL059069.

Mouginot, J., B. Scheuchl, and E. Rignot. 2012. Mapping of Ice Motion in Antarctica Using Synthetic-Aperture Radar Data. *Remote Sensing* 4(9): 2753-2767. doi: 10.3390/rs4092753.

Rignot, E., S. Jacobs, J. Mouginot, and B. Scheuchl. 2013. Ice Shelf Melting Around Antarctica. *Science* 341(6143): 266-270. doi: 10.1126/science.1235798.

Rignot, E., J. Mouginot, and B. Scheuchl. 2011. Ice Flow of the Antarctic Ice Sheet. *Science* 333(6048): 1427-1430. doi: 10.1126/science.1208336.

Rignot, E., J. Mouginot, and B. Scheuchl. 2011. Antarctic grounding line mapping from differential satellite radar interferometry. *Geophysical Research Letters* 38(10): Art. #L10504. doi: 10.1029/2011GL047109.

Rignot, E., J. L. Bamber, M. R. Van Den Broeke, C. Davis, Y. H. Li, W. J. Van De Berg, and E. Van Meijgaard. 2008. Recent Antarctic ice mass loss from radar interferometry and regional climate modelling. *Nature Geoscience* 1(2): 106-110. doi: 10.1038/ngeo102.

Scheuchl, B., J. Mouginot, and E. Rignot. 2012. Ice velocity changes in the Ross and Ronne sectors observed using satellite radar data from 1997 and 2009. *The Cryosphere* 6: 1019-1030. doi: 10.5194/tc-6-1019-2012.

3.3.1   RELATED DATA COLLECTIONS

- MEaSUREs Antarctic Grounding Line from Differential Satellite Radar Interferometry
- MEaSUREs InSAR-Based Ice Velocity Maps of Central Antarctica: 1997 and 2009
- MEaSUREs InSAR-Based Ice Velocity of the Amundsen Sea Embayment, Antarctica
- MEaSUREs Antarctic Boundaries for IPY 2007-2009 from Satellite Radar

3.3.2   RELATED WEB SITES

- NASA MEaSUREs Data at NSIDC
- NASA MEaSUREs

3.4 Contacts and Acknowledgments

Investigators

Dr. Eric Rignot
University of California, Irvine
Department of Earth System Science
Croul Hall
Irvine, California 92697
USA

Dr. Jeremie Mouginot
University of California, Irvine
Department of Earth System Science
Croul Hall
Irvine, California 92697
USA

Dr. Bernd Scheuchl
University of California, Irvine
Department of Earth System Science
Croul Hall

Irvine, California 92697

USA

3.4.1   Acknowledgments:

These data were generated through a grant from the NASA MEaSUREs program.

Spaceborne Synthetic Aperture Radar (SAR) acquisitions were provided through the following data agencies:

ALOS PALSAR: Japan Aerospace Exploration Agency (JAXA)

ENVISAT ASAR, ERS-1, ERS-2: European Space Agency (ESA)

Sentinel-1: Copernicus/ESA

RADARSAT-1, RADARSAT-2: Canadian Space Agency (CSA)

Landsat-8 (optical) data were made available by United States Geological Survey (USGS).

Data acquisitions between 2006 and 2016 are courtesy of the International Polar Year (IPY) Space Task Group and its successor, the Polar Space Task Group (PSTG).

Contains modified Copernicus Sentinel data (2014-2016), acquired by the European Space Agency, distributed through the Alaska Satellite Facility, and processed by Rignot, E., J. Mouginot, and B. Scheuchl.

4   DOCUMENT INFORMATION

4.1 Publication Date

April 2017

4.2 Date Last Updated

October 2020